

Duration of Individual Relativistic Electron Microbursts: A Probe Into Their Scattering Mechanism

M. Shumko^{1,2}, L.W. Blum³, and A.B. Crew⁴

¹NASA's Goddard Space Flight Center, Greenbelt, Maryland, USA

²Universities Space Research Association, Columbia, Maryland, USA

³University of Colorado Boulder, Boulder, Colorado, USA

⁴Johns Hopkins University Applied Physics Laboratory, Laurel, Maryland, USA

Key Points:

- We identified relativistic microbursts observed by the SAMPEX satellite and quantified their duration
- The microburst duration interquartile range is 70-140 ms and shows trends in AE, L-shell, and MLT
- In MLT, microburst durations double between midnight and noon—a trend similar to chorus element durations

Abstract

We used the Solar Anomalous and Magnetospheric Particle Explorer (SAMPEX) to identify and quantify the duration of relativistic, > 1 MeV, electron microbursts. A typical relativistic microburst has a ≈ 100 millisecond (ms) duration, and the interquartile range of the duration distribution is 70-140 ms. We investigated trends in the microburst duration as a function of geomagnetic activity, L-shell, and magnetic local time (MLT). The clearest trend is in MLT: the median microburst duration doubles from 80 milliseconds at midnight to 160 milliseconds noon MLT. This trend is similar to the whistler mode chorus rising tone element duration trend, suggesting a possible relationship.

Plain Language Summary

Energetic electron microbursts are an intense form of naturally occurring particle precipitation from the outer Van Allen Radiation Belt into Earth's atmosphere. Microbursts are observed in, or just above, the Earth's atmosphere, and are characterized by their short duration in time series data, often defined to be less than a second. The impact of microburst precipitation on the Earth's atmosphere is uncertain, but has been predicted to substantially degrade mesospheric ozone through the production of odd nitrogen and odd hydrogen molecules. Besides their environmental impact, we don't comprehensively understand how plasma waves, such as whistler mode chorus waves, scatter microbursts into our atmosphere. Therefore, in this study we quantified the duration of microbursts and used it as a proxy to understand how microbursts are scattered by these waves. We found that the microburst and chorus wave durations are correlated: their duration roughly doubles between the anti-sunward and sunward regions of the outer radiation belt.

1 Introduction

Earth's outer Van Allen radiation belt electron population is in constant flux, controlled by processes such as, radial transport, injections from the magnetotail, magnetopause shadowing, and local heating and loss into Earth's atmosphere due to wave-particle interactions (e.g. Ripoll et al., 2020, and references within). Whistler mode chorus is one type of plasma wave, characterized by subsecond rising tone elements, that plays a dual role in electron dynamics: accelerate electrons from 10s of keV to MeV energies, and pitch angle scatter electrons into the atmosphere (e.g. Li, Thorne, Angelopoulos, Bonnell, et al., 2009; Thorne, 2010; Horne & Thorne, 2003; Summers, 2005). One form of electron precipitation believed to be generated by chorus are microbursts: a subsecond intense increase of electrons. Microbursts were first observed by balloons in Earth's upper atmosphere, and later by satellites in low Earth orbit (LEO) (e.g. Winckler et al., 1962; Anderson & Milton, 1964; Blake et al., 1996; Lorentzen et al., 2001; O'Brien et al., 2003; Douma et al., 2017; Kurita et al., 2016), and recently at high altitude near the magnetic equator (Shumko et al., 2018).

Microburst electron energies span multiple orders of magnitude from tens of keV observed by, for example, Datta et al. (1997), to > 1 MeV observed by the Solar Anomalous Magnetospheric Particle Explorer (SAMPEX) by Blake et al. (1996). Microbursts are predominately observed outside the plasmapause on the outer radiation belt footprints, $L \approx 4 - 8$, and in the midnight to morning Magnetic Local Times (MLT) ($\approx 0-12$ hours MLT) (Lorentzen et al., 2001; Blum et al., 2015; O'Brien et al., 2003; Douma et al., 2017). While microbursts are observed under all geomagnetic conditions, Douma et al. (2017) showed that microburst occurrence frequency dramatically increases with the Auroral Electrojet (AE) index, and O'Brien et al. (2003) showed a similar trend with the microburst frequency with the Disturbance storm time index phase.

The relative impact of energetic electron precipitation on the ionization of Earth's atmosphere and the depletion of radiation belt electrons is uncertain, but is estimated to be substantial. Duderstadt et al. (2021) showed observations that suggest that electron precipitation can significantly impact atmospheric composition. The authors estimated a 20-30% increase in atmospheric odd nitrogen (NO_x), causing a 1% decrease in ozone (O_3)—substantial enough to affect the radiative balance in the upper atmosphere. Microbursts have also been estimated to be able to deplete the outer radiation belt electrons in hours to a few days, and models predict depletions of up to 20% of upper mesospheric O_3 (O'Brien et al., 2004; Thorne et al., 2005; Douma et al., 2019; Breneman et al., 2017; Seppälä et al., 2018).

Electron microbursts are widely believed to be scattered by chorus waves. They were associated early on, due to the similar duration of microbursts and chorus rising tone elements and a similar occurrence distributions in MLT and L-shell (e.g. Lorentzen et al., 2001). Furthermore, Breneman et al. (2017) ~~directly linked a chorus rising tone element to a microburst observed by the~~ associated chorus rising tone elements to microbursts observed by the Focused Investigation of Relativistic Electron Bursts: Intensity, Range, and Dynamics CubeSats (FIREBIRD-II; Crew et al. (2016); Johnson et al. (2020)) during a close magnetic conjunction.

A natural follow-on question is how are microbursts generated by chorus rising tone elements? For example, it is still unclear if relativistic (> 1 MeV) microbursts are scattered via cyclotron resonance at high magnetic latitudes, or a higher resonance harmonic near the magnetic equator (Lorentzen et al., 2001). One way to address this question is to study for how long microburst electrons are in resonance with a chorus wave. The resulting microburst duration, i.e. the microburst width in the time series data, is a probe into the conditions necessary to scatter microburst electrons. ~~Therefore, we used microbursts observed by the SAMPEX satellite to quantify the distribution of relativistic microburst durations. In this letter, we quantify the duration distribution of microbursts as a function of L-shell, MLT, and the Auroral Electrojet.~~ Thus, we used SAMPEX data to quantify the distribution of relativistic microburst durations as a function of L-shell, MLT, and the Auroral Electrojet index. We then compared these results to prior chorus rising tone element studies, and a chorus-electron test particle model.

2 Instrumentation

For this study we used the > 1 MeV electron data, taken by the Heavy Ion Large Telescope (HILT) instrument (Klecker et al., 1993) onboard the SAMPEX satellite (Baker et al., 1993). SAMPEX was launched in July 1992 and reentered Earth's atmosphere in November 2012. It was in a 520x670 km, 82° inclination low Earth orbit. In general, SAMPEX had two pointing modes: spin and orbit rate rotation (zenith pointing). To avoid the compounding effects due to the variable pitch angles sampled in the spin mode, we only used the zenith pointing mode data. The International Geomagnetic Reference Field (Thébault et al., 2015, IGRF) magnetic field model was used to derive the geomagnetic coordinates.

The HILT instrument consisted of a large rectangular chamber with the aperture on one end, and 16 solid state detectors on the other. We used the HILT electron data taken between 1997 and 2012 (state4 in the data archive). The electron counts were accumulated from all of the solid state detectors at a 20 ms cadence.

3 Methodology

~~We first identified microbursts. We then fit every microburst time series to a model, consisting of a Gaussian superposed with a straight line, to quantify the duration for each microburst.~~



Figure 1. Examples of relativistic microbursts are shown by the black curves, and the fits are shown by the dashed red curves. The fit’s full width at half maximum (FWHM) and the \bar{R}^2 goodness of fit metric is annotated in each panel. Microbursts with $\bar{R}^2 > 0.9$ were used for this study—hence the two-peaked example in panel a was not analyzed. The major time ticks are at every second, while the minor ticks are at every 100 milliseconds.

3.1 Microburst Identification

In the first step, we identified microbursts using the burst parameter defined by O’Brien et al. (2003), also used in numerous other SAMPEX microburst studies (e.g. Douma et al., 2017). Assuming Poisson probability for the observed electron counts, the burst parameter is the number of standard deviations of a foreground signal above the background, expressed as

$$n_{\sigma} = \frac{N - A}{\sqrt{A + 1}} \quad (1)$$

where N is the number of foreground electron counts, and A is the centered running average background counts. The 1 in the denominator prevents a division by 0 error. In O’Brien et al. (2003), and in the results in this study, N was summed over 100 ms and is called N_{100} , while A was summed over 500 ms and is likewise called A_{500} . Henceforth, we specify the time windows with subscripts for N and A . Times when $n_{\sigma} > 10$ are classified as burst times, and the peak time in each continuous burst time interval is saved to the microburst data set. With A_{500} and N_{100} , we detected a total of 256,764 microbursts over the 15 year period from 1997 to 2012. Four examples of microbursts are shown in Fig. 1 by the solid black curves.

3.2 Microburst Duration Quantification

In the second step, we estimated the microburst duration using two methods, detailed below, that yielded similar results: the duration at half of the microburst’s topographic prominence and the full width at half maximum (FWHM) from a Gaussian fit.

The topographic prominence is a simple and robust method to estimate the microburst duration previously used to identify curtains, a similar-looking type of precipitation (Shumko et al., 2020). [Using this technique, we define microburst duration to be](#) the duration at half of the microburst’s topographic prominence: the height of the microburst relative to the maximum of the two minima on either side of the microburst peak. On each side of the microburst peak, the minima are searched for between the microburst and a higher peak on that side. While the topographic prominence method of estimating microburst durations is simple and robust, a downside is its inability to automatically verify that the estimated duration is of a single microburst and not a superposition of multiple microbursts (Fig. 1a [is an example of two superposed microbursts](#)).

Therefore, we also fit microbursts with a Gaussian, and used the R^2 goodness of fit metric to exclude bad duration estimates such as a superposition of multiple microbursts one potential source of bias.

To overcome this downside, we fit the microburst time series and used the R^2 goodness of fit metric to verify the fit. We assumed a fit model consisting of a Gaussian superposed with a straight line for the background counts at and around the microburst. The Gaussian models the shape of the microburst and the linear trend models the background electrons that are either trapped or quasi-trapped in the drift loss cone. This model is defined as

$$c(t|A, t_0, \sigma, c_0, c_1) = Ae^{-\frac{(t-t_0)^2}{2\sigma^2}} + c_0 + c_1t \quad (2)$$

where A , t_0 , and σ are the Gaussian amplitude, center time, and standard deviation; c_0 and c_1 are the linear background count intercept and slope. The fit time interval is We determined the number of data points to fit as the maximum of: 4x topographic prominence duration or 500 ms. A challenge to any robust and automated nonlinear regression algorithm is guessing the initial parameters. The initial parameter guesses for the Gaussian are provided by the estimated topographic prominence and duration. The straight line parameter guesses were: $c_0 = \text{median}(\text{counts})$ and $c_1 = 0$. The optimal fit parameters were found using `scipy's curve_fit()` function in Python. We defined the microburst duration as the FWHM of the microburst peak, defined by

$$\text{FWHM} = 2\sqrt{2\ln 2}\sigma. \quad (3)$$

To evaluate the fit, we used the R^2 goodness of fit metric. R^2 is defined as

$$R^2 = 1 - \frac{SS_{res}}{SS_{mean}} = 1 - \frac{\sum (c_i - f_i)^2}{\sum (c_i - \bar{c})^2} \quad (4)$$

where SS_{res} is the sum of the squared residuals between the observed counts c_i and the fit counts f_i for each time step, and likewise SS_{mean} is the sum of the squared residuals between c_i and the mean of the counts, \bar{c} .

One interpretation of R^2 is fractionally how much better the variance in the data is explained by the model fit, compared to the null hypothesis horizontal line at \bar{c} . R^2 varies from 1 for a perfect fit that perfectly describes the data, to $-\infty$ for poor fits (a fit can be much worse than the mean null hypothesis).

To account for overfitting, we used the adjusted R^2 , \bar{R}^2 , defined as

$$\bar{R}^2 = 1 - (1 - R^2) \frac{n - 1}{n - p - 1} \quad (5)$$

where n is the number of data points fit, and p is the number of parameters. Intuitively, $n - 1$ is the number of degrees of freedom for the null hypothesis, and $n - p - 1$ is the degrees of freedom for the fit model. Fits with $\bar{R}^2 > 0.9$ are considered good and are analyzed. As a check, we compared the microburst duration estimated with the prominence and fit methods. We first chose an agreement criterion between the two methods as a duration within 25%; together with the $\bar{R}^2 > 0.9$ constraint, 85% of microbursts satisfied this criterion these criteria.

Figure 1a shows an example of two superposed microbursts that had a fit $\bar{R}^2 = 0.83$ that were excluded from this study. On other hand, microbursts in Fig. 1b-d had $\bar{R}^2 > 0.9$ and were included in the following analysis. Lastly, Fig. 1c and d demonstrate the necessity of the linear fit to account for the changing background. The linear fit accounts for the non-zero mean background counts and the uneven amplitudes at the edges of the Gaussian. Of the 256,764 detected microbursts, 109,231 have $\bar{R}^2 > 0.9$ and are used for the remainder of this study.

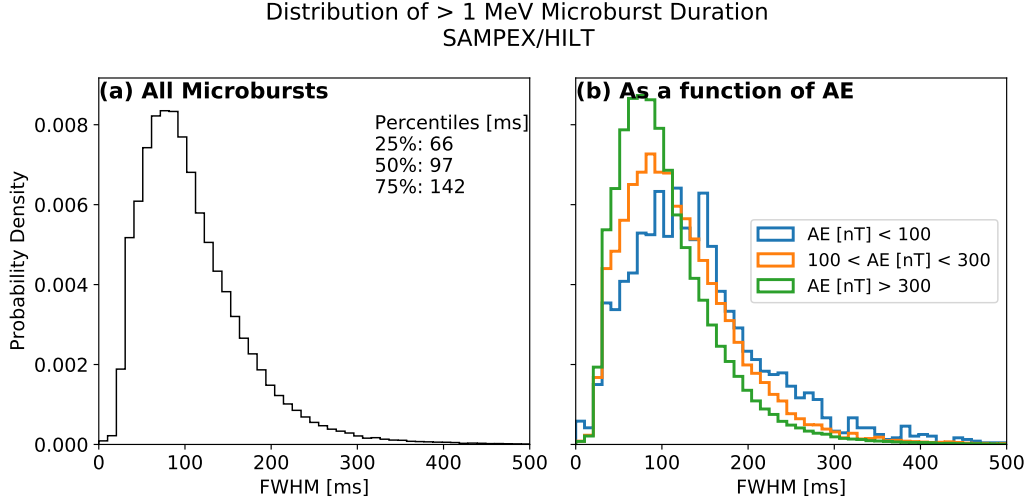


Figure 2. Panel a shows the distribution of all microburst full width at full maximum (FWHM). Panel b shows the distribution of all microbursts, categorized by the Auroral Electrojet (AE) index into three bins: $AE < 100$, $100 < AE < 300$, and $AE > 300$, in units of nT. The median microburst duration is 130 ms for the $AE < 100$ (2.4×10^3 microbursts), 111 ms for the $100 < AE < 300$ (1.8×10^4 microbursts), and 95 ms for the $AE > 300$ (9.3×10^4 microbursts) bins.

4 Results

We used the well-fit microbursts to quantify the distribution of microburst duration (FWHM). We then investigated trends in the duration distribution as a function of the Auroral Electrojet index, L-shell and MLT. We begin with the overall microburst distribution.

Figure 2a shows the distribution of all well-fit microbursts. This distribution is strongly peaked with 97 ms median duration. The interquartile range spans about a factor of two in microburst duration, from 66 to 142 ms.

We then investigated the dependence of microburst duration as a function of geomagnetic activity. To be consistent with many prior wave and microburst studies, we use the AE index to quantify the level of geomagnetic disturbance. We adopt the same three AE intensity levels used in prior studies, such as Douma et al. (2017), and Meredith et al. (2020): $AE < 100$, $100 < AE < 300$, and $AE > 300$, in units of nanotesla (nT). Figure 2b shows the distribution of microburst duration for the three AE categories. The distributions are qualitatively similar, gradually narrowing and shifting to shorter durations with increasing AE. The median microburst duration decreases from 130 ms for $AE < 100$ to 95 ms for $AE > 300$.

Lastly, Figs. 3 and 4 show the microburst duration as a function of L and MLT. Figure 3a shows the joint distributions, split up into the 25th, 50th, and 75th percentiles shows the median microburst distribution, while Figure 4 shows the marginalized distributions as a function of L or MLT. Figure 3 shows that the microburst duration trend is nearly identical for the different percentiles, and thus for simplicity we focus on the median distribution in Fig. 3b. The median microburst duration trend in Fig. 3a roughly doubles: from 80 ms at midnight to 160 ms at noon. In L-shell, the median microburst duration slightly increases with L-shell, most apparent near midnight MLT.

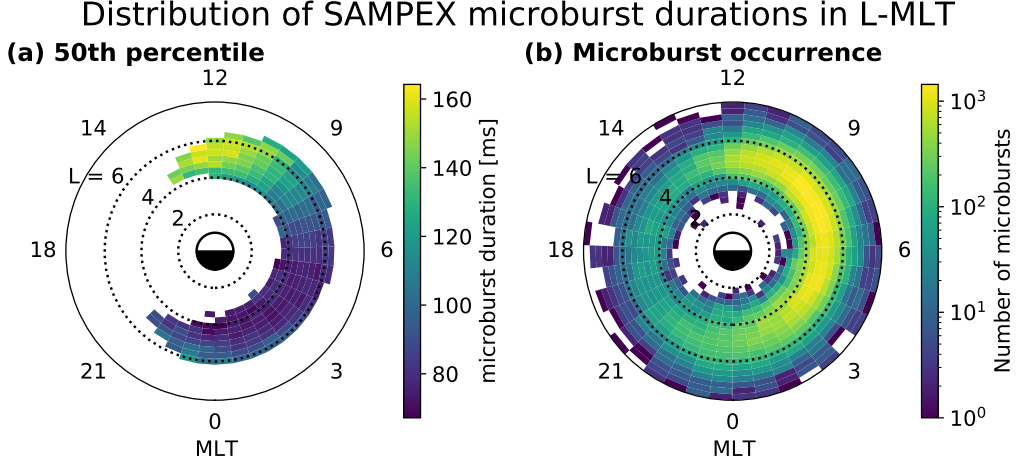


Figure 3. Panel a shows the joint distribution of the median microburst duration (FWHM) as a function of L-Shell and MLT. The white bins in panel a have less than 100 microbursts and are statistically insufficient. Panel b shows the distribution of the number of microbursts, with the white bins containing 0 microbursts.

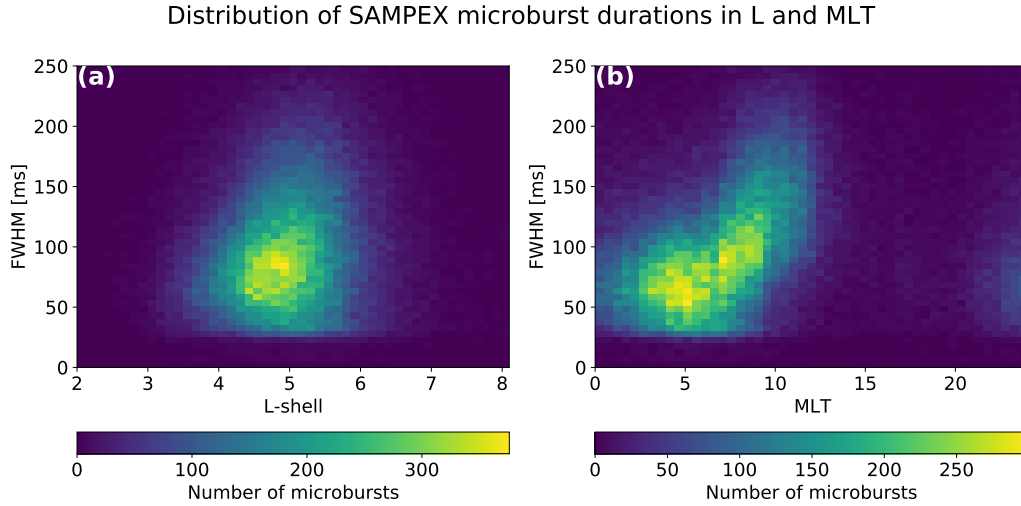


Figure 4. The marginalized distributions of the number of microbursts as a function of microburst duration (FWHM) and L shell in panel a, and MLT in panel b.

To disentangle the L and MLT distributions, Fig. 4 shows the marginalized distributions; MLT was marginalized out (summed over) in Fig. 4a and L-shell was marginalized out in Fig. 4b. Figure 4a shows a slight broadening of the microburst duration at higher L-shells—in contrast to Fig. 4b, that clearly shows the microburst duration increase from midnight to noon MLT.

5 Discussion and Conclusions

We found that > 1 MeV microbursts have a duration distribution peaked at ≈ 100 ms, with 50% of microburst durations between 66 – 142 ms. Microburst durations slightly shrink with increasing AE index and slightly grow with increasing L. We

found a significant trend in MLT—the median microburst duration doubles from 80 to 160 ms between midnight and noon MLT. However, before we put these results in the larger context, we first need to understand how our choice of microburst detection algorithm can lead to reduced sensitivity to microbursts that are longer than ≈ 200 ms.

We first discuss a possibility that the burst detection parameter is less sensitive to microbursts with longer durations, artificially restricting the upper limit of microburst durations detected in this study. Recall from Section 3.1 that A is the running average counts, centered on the foreground counts N , and the burst parameter, $n_\sigma \sim N - A$. Now consider the following hypothesized scenario. Given a microburst with a 500 ms duration and the burst parameter centered on the peak, A_{500} completely overlaps with the microburst and is therefore the mean microburst counts. Then, n_σ is proportional to the difference between the mean and the maximum microburst amplitude. However, if we use A_{1000} , it no longer overlaps with just the microburst, but rather the microburst and the lower surrounding background. The resulting A_{1000} is lower than A_{500} —thus the A_{1000} burst parameter is more sensitive to the microburst.

To test this possible bias, we ran the detection algorithm with three background values: A_{500} , A_{1000} , and A_{2000} and compared the resulting median distributions. The maximum discrepancy in the median microburst duration, using the three resulting data sets, was 20 ms—one HILT time sample. This is a 20% relative discrepancy. Consequently, considering this bias and the distribution in Fig. 2a, the evidence supports that the majority of > 1 MeV microbursts have a true duration around 100 ms and the A_{500} is adequate to identify them. With more confidence in the detection algorithm, we now discuss the global distribution of microburst durations.

The microburst duration trend in L-shell is subtle: the median microburst duration increases from 85 to 106 ms between $L=4$ and 5.5 and then decreases to 90 ms at $L=7$. This subtle trend is most evident in Fig. 4a. In contrast, the duration trend in MLT is significant. Figure 4b shows that the median microburst duration doubles from 80 to 160 ms between midnight and noon MLT. Now we will focus on the MLT trend and look for a possible explanation.

As mention in the introduction, chorus rising tone elements are widely believed to scatter microburst electrons (e.g. Breneman et al., 2017; Saito et al., 2012; Miyoshi et al., 2020). Thus, we will compare the microburst duration and chorus trends in local time. Recent studies by Teng et al. (2017) and Shue et al. (2019) quantified the properties of equatorial lower band (0.1-0.5 x electron gyrofrequency) chorus rising tone elements. Both studies found that the rising tone element duration distribution peaks at ≈ 250 ms around midnight, and broadening and shifting to ≈ 500 ms at noon. The microburst and chorus rising tone element durations double between midnight and noon MLT, but the chorus rising tone element duration is roughly 3 times longer than the relativistic microbursts. The previous chorus duration results and our microburst duration results both found that their durations roughly double from midnight to noon MLT. However, the chorus durations are about 3-4x longer than the microbursts. This scaling is consistent with Miyoshi et al. (2020) who predicted a similar difference in duration between chorus rising tone element and relativistic microburst durations.

As a function of AE, the median microburst duration decreases from 130 ms, for $AE < 100$ nT, to 95 ms for $AE > 300$ nT. The chorus rising tone duration trend, quantified by Teng et al. (2017), is similar: it is broad and peaks at ≈ 500 ms for $AE < 100$ nT, then narrows and shifts to ≈ 250 ms for $AE > 300$ nT. While both become shorter with increased AE, the scaling factors are different. the change in microburst duration is relatively smaller than the change in chorus duration.

Numerous test particle simulations have been performed to study the relationship between chorus rising tone elements and microbursts. Chen et al. (2020) found that medium energy ($\approx 50 - 300$ keV) microburst duration is controlled by the rising tone element bandwidth. Moreover, higher energy microburst duration is controlled by the wave's lower frequency and the absolute value of the upper magnetic latitude of propagation. Their results are in qualitative agreement with the cyclotron resonance condition described in Lorentzen et al. (2001), and the simulated electron time of flight described by Saito et al. (2012).

While different model configurationsparameters may change what wave properties are theoretically responsible for scattering > 1 MeV microburst electrons, it is worth noting that Figs. 4 and 5 in Shue et al. (2019) do not show a clear shift in chorus bandwidth between midnight and noon MLT. Care must be taken when comparing our results to theory: HILT measured multi-energy microburst electrons above 1 MeV, and microbursts at each energy can have different drivers and durations, as simulated by Chen et al. (2020) and Miyoshi et al. (2020). Nevertheless, theory does not conclusively predict what chorus wave properties control the > 1 MeV microburst duration, but the chorus rising tone duration trend in MLT is worth further consideration.

Lastly, high latitude chorus waves, found at $|\lambda| \approx 10^\circ - 25^\circ$ magnetic latitude off of the equator, can also play an important role at scattering microburst electrons (Lorentzen et al., 2001). Li, Thorne, Angelopoulos, Bortnik, et al. (2009) found that the majority of high latitude chorus waves are constrained to 6-12 MLT. Thus, it is tempting to conclude that the microburst duration trend in MLT could be attributed to some difference in how low and high latitude chorus waves scatter MeV electrons. However, because low latitude chorus waves are also observed at 0-12 MLT, the resulting microburst duration distribution would reflect the chorus wave superposition in the 6-12 MLT region. If low and high latitude chorus waves scattered microbursts with different durations, Fig. 4b would show the microburst durations broaden or bifurcate from midnight to noon MLT. Because Fig. 4b shows the entire microburst duration distribution shifting to longer durations, high vs low latitude chorus waves are an unlikely explanation for the microburst duration trend in MLT.

In summary, we found that the relativistic microburst duration distribution is peaked at 100 ms, with 75% of microbursts narrower than 140 ms. We discovered a strong trend in microburst duration as a function of MLT—the median microburst duration roughly doubling from 80 ms at midnight, to 160 ms at noon. ~~We found that both the microburst and chorus rising tone element durations double in MLT.~~ Prior work also shows that chorus rising tone element durations double in MLT; in a given local time the rising tone element duration is longer. These results indicate a likely relationship between durations of chorus rising tone elements and microbursts, and we encourage future modeling work to explore this relationship.

Acknowledgments

We are thankful for the engineers and scientists who made the SAMPEX mission possible. M. Shumko acknowledges the support provided by the NASA Postdoctoral Program at the NASA's Goddard Space Flight Center, administered by Universities Space Research Association under contract with NASA; L.W.Blum acknowledges the Heliophysics Innovation Fund program at NASA's Goddard Space Flight Center; and A.B. Crew acknowledges funding provided by the National Science Foundation, award 1602607. The SAMPEX HILT and attitude data are located at <http://www.srl.caltech.edu/sampex/DataCenter/data.html> and the minute cadence Auroral Electrojet data is located at ftp://ftp.ngdc.noaa.gov/STP/GEOMAGNETIC_DATA/INDICES/AURORAL_ELECTROJET/ONE_MINUTE/. This analysis software is available at: https://github.com/mshumko/sampex_microburst_widths, and is archived on Zenodo <https://doi.org/10.5281/zenodo.4687987>

References

- Anderson, K. A., & Milton, D. W. (1964). Balloon observations of X rays in the auroral zone: 3. High time resolution studies. *Journal of Geophysical Research*, 69(21), 4457–4479. Retrieved from <http://dx.doi.org/10.1029/JZ069i021p04457> doi: 10.1029/JZ069i021p04457
- Baker, D. N., Mason, G. M., Figueroa, O., Colon, G., Watzin, J. G., & Aleman, R. M. (1993). An overview of the solar anomalous, and magnetospheric particle explorer (SAMPEX) mission. *IEEE Transactions on Geoscience and Remote Sensing*, 31(3), 531–541.
- Blake, J. B., Looper, M. D., Baker, D. N., Nakamura, R., Klecker, B., & Hovestadt, D. (1996). New high temporal and spatial resolution measurements by sampex of the precipitation of relativistic electrons. *Advances in Space Research*, 18(8), 171 - 186. Retrieved from <http://www.sciencedirect.com/science/article/pii/0273117795009698> doi: [http://dx.doi.org/10.1016/0273-1177\(95\)00969-8](http://dx.doi.org/10.1016/0273-1177(95)00969-8)
- Blum, L., Li, X., & Denton, M. (2015). Rapid MeV electron precipitation as observed by SAMPEX/HILT during high-speed stream-driven storms. *Journal of Geophysical Research: Space Physics*, 120(5), 3783–3794. Retrieved from <http://dx.doi.org/10.1002/2014JA020633> (2014JA020633) doi: 10.1002/2014JA020633
- Breneman, A., Crew, A., Sample, J., Klumpar, D., Johnson, A., Agapitov, O., ... others (2017). Observations directly linking relativistic electron microbursts to whistler mode chorus: Van allen probes and FIREBIRD II. *Geophysical Research Letters*.
- Chen, L., Breneman, A. W., Xia, Z., & Zhang, X.-j. (2020). Modeling of bouncing electron microbursts induced by ducted chorus waves. *Geophysical Research Letters*, 47(17), e2020GL089400. Retrieved from <https://agupubs.onlinelibrary.wiley.com/doi/abs/10.1029/2020GL089400> (e2020GL089400 10.1029/2020GL089400) doi: <https://doi.org/10.1029/2020GL089400>
- Crew, A. B., Spence, H. E., Blake, J. B., Klumpar, D. M., Larsen, B. A., O'Brien, T. P., ... Widholm, M. (2016). First multipoint in situ observations of electron microbursts: Initial results from the NSF FIREBIRD II mission. *Journal of Geophysical Research: Space Physics*, 121(6), 5272–5283. Retrieved from <http://dx.doi.org/10.1002/2016JA022485> (2016JA022485) doi: 10.1002/2016JA022485
- Datta, S., Skoug, R., McCarthy, M., & Parks, G. (1997). Modeling of microburst electron precipitation using pitch angle diffusion theory. *Journal of Geophysical Research: Space Physics*, 102(A8), 17325–17333.
- Douma, E., Rodger, C., Blum, L., O'Brien, T., Clilverd, M., & Blake, J. (2019). Characteristics of relativistic microburst intensity from sampex observations. *Journal of Geophysical Research: Space Physics*.
- Douma, E., Rodger, C. J., Blum, L. W., & Clilverd, M. A. (2017). Occurrence characteristics of relativistic electron microbursts from SAMPEX observations. *Journal of Geophysical Research: Space Physics*, 122(8), 8096–8107. Retrieved from <http://dx.doi.org/10.1002/2017JA024067> (2017JA024067) doi: 10.1002/2017JA024067
- Duderstadt, K. A., Huang, C.-L., Spence, H. E., Smith, S., Blake, J. B., Crew, A. B., ... Vitt, F. M. (2021). Estimating the impacts of radiation belt electrons on atmospheric chemistry using firebird ii and van allen probes observations. *Journal of Geophysical Research: Atmospheres*, n/a(n/a), e2020JD033098. Retrieved from <https://agupubs.onlinelibrary.wiley.com/doi/abs/10.1029/2020JD033098> (e2020JD033098 2020JD033098) doi: <https://doi.org/10.1029/2020JD033098>
- Horne, R. B., & Thorne, R. M. (2003). Relativistic electron acceleration and pre-

- 372 cipitation during resonant interactions with whistler-mode chorus. *Geophysi-*
 373 *cal Research Letters*, 30(10). Retrieved from [http://dx.doi.org/10.1029/](http://dx.doi.org/10.1029/2003GL016973)
 374 2003GL016973 (1527) doi: 10.1029/2003GL016973
- 375 Johnson, A., Shumko, M., Griffith, B., Klumpar, D., Sample, J., Springer, L., ...
 376 others (2020). The FIREBIRD-II CubeSat mission: Focused investigations of
 377 relativistic electron burst intensity, range, and dynamics. *Review of Scientific*
 378 *Instruments*, 91(3), 034503.
- 379 Klecker, B., Hovestadt, D., Scholer, M., Arbing, H., Ertl, M., Kastele, H., ... oth-
 380 ers (1993). HILT: A heavy ion large area proportional counter telescope for
 381 solar and anomalous cosmic rays. *IEEE transactions on geoscience and remote*
 382 *sensing*, 31(3), 542–548.
- 383 Kurita, S., Miyoshi, Y., Blake, J. B., Reeves, G. D., & Kletzing, C. A. (2016). Rel-
 384 ativistic electron microbursts and variations in trapped mev electron fluxes
 385 during the 8–9 october 2012 storm: Sampex and van allen probes observations.
 386 *Geophysical Research Letters*, 43(7), 3017-3025. Retrieved from [https://](https://agupubs.onlinelibrary.wiley.com/doi/abs/10.1002/2016GL068260)
 387 [agupubs.onlinelibrary.wiley.com/doi/abs/10.1002/2016GL068260](https://doi.org/10.1002/2016GL068260) doi:
 388 <https://doi.org/10.1002/2016GL068260>
- 389 Li, W., Thorne, R., Angelopoulos, V., Bonnell, J., McFadden, J., Carlson, C., ...
 390 Auster, H. (2009). Evaluation of whistler-mode chorus intensification on
 391 the nightside during an injection event observed on the THEMIS spacecraft.
 392 *Journal of Geophysical Research: Space Physics*, 114(A1).
- 393 Li, W., Thorne, R. M., Angelopoulos, V., Bortnik, J., Cully, C. M., Ni, B., ...
 394 Magnes, W. (2009). Global distribution of whistler-mode chorus waves ob-
 395 served on the THEMIS spacecraft. *Geophysical Research Letters*, 36(9).
 396 Retrieved from <http://dx.doi.org/10.1029/2009GL037595> (L09104) doi:
 397 10.1029/2009GL037595
- 398 Lorentzen, K. R., Blake, J. B., Inan, U. S., & Bortnik, J. (2001). Observations of
 399 relativistic electron microbursts in association with VLF chorus. *Journal of*
 400 *Geophysical Research: Space Physics*, 106(A4), 6017–6027. Retrieved from
 401 <http://dx.doi.org/10.1029/2000JA003018> doi: 10.1029/2000JA003018
- 402 Meredith, N. P., Horne, R. B., Shen, X.-C., Li, W., & Bortnik, J. (2020). Global
 403 model of whistler mode chorus in the near-equatorial region ($|\lambda_m| < 18^\circ$). *Geo-*
 404 *physical Research Letters*, 47(11), e2020GL087311.
- 405 Miyoshi, Y., Saito, S., Kurita, S., Asamura, K., Hosokawa, K., Sakanoi, T., ... oth-
 406 ers (2020). Relativistic electron microbursts as high energy tail of pulsating
 407 aurora electrons.
- 408 O'Brien, T. P., Looper, M. D., & Blake, J. B. (2004). Quantification of relativis-
 409 tic electron microburst losses during the GEM storms. *Geophysical Research*
 410 *Letters*, 31(4). Retrieved from <http://dx.doi.org/10.1029/2003GL018621>
 411 (L04802) doi: 10.1029/2003GL018621
- 412 O'Brien, T. P., Lorentzen, K. R., Mann, I. R., Meredith, N. P., Blake, J. B., Fen-
 413 nell, J. F., ... Anderson, R. R. (2003). Energization of relativistic elec-
 414 trons in the presence of ULF power and MeV microbursts: Evidence for dual
 415 ULF and VLF acceleration. *Journal of Geophysical Research: Space Physics*,
 416 108(A8). Retrieved from <http://dx.doi.org/10.1029/2002JA009784> doi:
 417 10.1029/2002JA009784
- 418 Ripoll, J.-F., Claudepierre, S., Ukhorskiy, A., Colpitts, C., Li, X., Fennell, J., &
 419 Crabtree, C. (2020). Particle dynamics in the earth's radiation belts: Review
 420 of current research and open questions. *Journal of Geophysical Research: Space*
 421 *Physics*, 125(5), e2019JA026735.
- 422 Saito, S., Miyoshi, Y., & Seki, K. (2012). Relativistic electron microbursts as-
 423 sociated with whistler chorus rising tone elements: Gensis-rbw simulations.
 424 *Journal of Geophysical Research: Space Physics*, 117(A10), n/a–n/a. Re-
 425 trieved from <http://dx.doi.org/10.1029/2012JA018020> (A10206) doi:
 426 10.1029/2012JA018020

- 427 Seppälä, A., Douma, E., Rodger, C., Verronen, P., Clilverd, M. A., & Bortnik, J.
428 (2018). Relativistic electron microburst events: Modeling the atmospheric
429 impact. *Geophysical Research Letters*, 45(2), 1141–1147.
- 430 Shue, J.-H., Nariyuki, Y., Katoh, Y., Saito, S., Kasahara, Y., Hsieh, Y.-K., ... Goto,
431 Y. (2019). A systematic study in characteristics of lower band rising-tone
432 chorus elements. *Journal of Geophysical Research: Space Physics*, 124(11),
433 9003–9016.
- 434 Shumko, M., Johnson, A. T., O'Brien, T. P., Turner, D. L., Greeley, A. D., Sam-
435 ple, J. G., ... Halford, A. J. (2020). Statistical properties of electron cur-
436 tain precipitation estimated with aerocube-6. *Journal of Geophysical Re-*
437 *search: Space Physics*, 125(12), e2020JA028462. Retrieved from [https://](https://agupubs.onlinelibrary.wiley.com/doi/abs/10.1029/2020JA028462)
438 agupubs.onlinelibrary.wiley.com/doi/abs/10.1029/2020JA028462
439 (e2020JA028462 10.1029/2020JA028462) doi: [https://doi.org/10.1029/](https://doi.org/10.1029/2020JA028462)
440 2020JA028462
- 441 Shumko, M., Turner, D. L., O'Brien, T. P., Claudepierre, S. G., Sample, J.,
442 Hartley, D. P., ... Mitchell, D. G. (2018). Evidence of microbursts ob-
443 served near the equatorial plane in the outer van allen radiation belt. *Geo-*
444 *physical Research Letters*, 45(16), 8044-8053. Retrieved from [https://](https://agupubs.onlinelibrary.wiley.com/doi/abs/10.1029/2018GL078451)
445 agupubs.onlinelibrary.wiley.com/doi/abs/10.1029/2018GL078451 doi:
446 10.1029/2018GL078451
- 447 Summers, D. (2005). Quasi-linear diffusion coefficients for field-aligned electro-
448 magnetic waves with applications to the magnetosphere. *Journal of Geophys-*
449 *ical Research: Space Physics*, 110(A8), n/a–n/a. Retrieved from [http://dx](http://dx.doi.org/10.1029/2005JA011159)
450 [.doi.org/10.1029/2005JA011159](http://dx.doi.org/10.1029/2005JA011159) (A08213) doi: 10.1029/2005JA011159
- 451 Teng, S., Tao, X., Xie, Y., Zonca, F., Chen, L., Fang, W., & Wang, S. (2017). Anal-
452 ysis of the duration of rising tone chorus elements. *Geophysical Research Let-*
453 *ters*, 44(24), 12–074.
- 454 Thébault, E., Finlay, C. C., Beggan, C. D., Alken, P., Aubert, J., Barrois, O., ...
455 others (2015). International geomagnetic reference field: the 12th generation.
456 *Earth, Planets and Space*, 67(1), 79.
- 457 Thorne, R. M. (2010). Radiation belt dynamics: The importance of wave-particle in-
458 teractions. *Geophysical Research Letters*, 37(22). Retrieved from [http://dx](http://dx.doi.org/10.1029/2010GL044990)
459 [.doi.org/10.1029/2010GL044990](http://dx.doi.org/10.1029/2010GL044990) (L22107) doi: 10.1029/2010GL044990
- 460 Thorne, R. M., O'Brien, T. P., Shprits, Y. Y., Summers, D., & Horne, R. B. (2005).
461 Timescale for MeV electron microburst loss during geomagnetic storms. *Jour-*
462 *nal of Geophysical Research: Space Physics*, 110(A9). Retrieved from [http://](http://dx.doi.org/10.1029/2004JA010882)
463 dx.doi.org/10.1029/2004JA010882 (A09202) doi: 10.1029/2004JA010882
- 464 Winckler, J., Bhavsar, P., & Anderson, K. (1962). A study of the precipitation of
465 energetic electrons from the geomagnetic field during magnetic storms. *Journal*
466 *of Geophysical Research*, 67(10), 3717–3736.